Topology analysis of global and local RBF transformations for image registration

Topology analysis of global and local RBF transformations for image registration

Roberto Cavoretto, Alessandra De Rossi, Hanli Qiao

Department of Mathematics "G. Peano", University of Torino, via Carlo Alberto 10, I–10123 Torino, Italy

Abstract

For elastic registration, topology preservation is a necessary condition to be satisfied, especially for landmark-based image registration. In this paper, we focus on the topology preservation properties of two different families of radial basis functions (RBFs), known as Gneiting and Matérn functions. Firstly, we consider a small number of landmarks, dealing with the cases of one, two and four landmark matching; in all these situations we analyze topology preservation and compare numerical results with those obtained by Wendland functions. Secondly, we discuss the registration properties of these two families of functions, when we have a larger number of landmarks. Finally, we analyze the behaviour of Gneiting and Matérn functions, considering some test examples known in the literature and a real application.

Keywords: Scattered data interpolation, Gneiting functions, Matérn functions, landmark-based image registration, topology preservation.
2010 MSC: 65D05, 65D07, 68U10.

1. Introduction

Image registration is a crucial step to get on further research in many scientific fields, such as medical image processing, image fusion and remote sensing. In medical images, 2D and 3D registrations are necessary in order to observe the evolution of a pathology or make full use of advantages of the complementary information. There are many references that deal with the role of registration and its applications in medical image processing, for an overview, see [29, 27, 23, 12]. Moreover, specific applications to medical image registration involving Magnetic Resonance Imaging (MRI) and Computer Tomography (CT) are considered in [23, 12, 31, 30]. Registration is also one of the basic stages of image fusion, which is the process of combining multiple information from a set of images. Effective image fusion can usually be fulfilled after accurate registration; in particular, in [20, 26, 4, 21] some applications of registration in image fusion with related connections are analyzed from different viewpoints. For remote sensing, registration is the first step on use of remote sensed images, see [11, 19, 15]. Hence, research for image registration is meaningful and necessary in many real-life applications. More specifically, in image registration we study the differences between a pair of images, where the objects are placed in the same scene but they are analyzed considering different periods of time, devices and/or perspectives, see [6, 28, 32, 33, 38] for a survey. In [24] Maintz and Viergever classify registration methods by nine criteria formulated in [35]. The classical problem of registration consists in finding an appropriate transformation between two data sets. A lot of techniques can solve this problem, and in [33] we can find a detailed description of the mathematical and computational methods used. From [38] we know that the main techniques of image registration should consider four steps, i.e., feature detection and matching, transform model estimation, image resampling and transformation. In the third step, a mapping by Radial Basis Functions (RBFs), which initially were applied for interpolation of irregular surfaces, is introduced. The word "radial" stands for the property that values of these functions at each point only depend on the distances from their center points rather than the specific locations [7, 14, 36]. This feature can be used to express the deformation for landmark

Email addresses: roberto.cavoretto@unito.it (Roberto Cavoretto), alessandra.derossi@unito.it (Alessandra De Rossi), hanli.qiao@unito.it (Hanli Qiao)

based image registration, and each landmark can be deemed as their center. A variety of RBFs has been studied for elastic image registration and deformation, and thin plate spline, multiquadrics, inverse multiquadrics and Gaussian functions are analytically been compared from viewpoints of locality, solvability and efficiency. Nevertheless, all these RBFs have no compact supports, hence if one landmark changes the whole registration result might also be subjected to a significant change. This is a drawback for a very local deformation of images. However, the use of Compactly Supported Radial Basis Functions (CSRBFs) can overcome this disadvantage. In particular, in [16] the use of Wendland functions in image registration is introduced, while in [1, 8, 9] other techniques involving compactly supported basis functions, such as Gneiting functions, were applied and the numerical results were compared with those obtained by Wendland functions. Results show that Gneiting functions have lower errors and smoother transformed images, also in real-life cases. Moreover, Gneiting functions have better performance with fixed parameter than other CSRBFs.

For an elastic transformation scheme, topology preservation is a major requirement. In [37] topology preservation of various CSRBFs is analyzed in three cases, i.e., one, two and four landmark matching. In this paper, we evaluate the topology preservation of Gneiting and Matérn functions. Although Matérn functions are well known in the statistics literature [13, 25, 34], as far as we know, excepting [10], there is no work focuses on applying them to image registration. We study and evaluate the properties of such functions in topology preservation based on a small number of landmarks. Specifically, we analyze topology preservation using two criteria: the locality parameter of the RBFs and the positivity of the determinant of Jacobian matrix. Moreover, for the different transformations we also compute the errors committed. In addition, we study their behaviour focusing on a larger number of landmarks in case of landmark shift, scaling, contraction and expansion, and finally we compare the numerical results with the ones obtained by standard techniques, such as Wendland functions. Furthermore, we analyze and compare the performance of some RBFs in real medical images. In particular, we report some registration results, showing the applicability to a real case and discussing the different possible choices of the shape parameter associated with the RBFs.

The paper is arranged as follows. In Section 2, we introduce two kinds of Gneiting and three examples of Matérn functions. Sections 3-5 give the analysis about the topology preservation under the two criteria mentioned above, dealing with the cases of one, two and four landmark matching, respectively. We also show some numerical results of Gneiting and Matérn functions and compare them with Wendland functions. In Section 6 we evaluate the performances of Gneiting and Matérn functions in four test cases, shift and scaling of a square and contraction and expansion of a circle, using a large number of landmarks. Section 7 deals with a real MRI application. Finally, in Section 8 some conclusions are given.

2. Gneiting and Matérn functions

In this paper, we consider 2D registration case. At first, we briefly introduce the transformation scheme of image registration based on landmarks. Given a set of source landmark points $\mathcal{S}_N=\{\mathbf{x}_j \in \mathbb{R}^2, j = 1, 2, \ldots, N\}$, and the corresponding pair of target landmark points $\mathcal{T}_N=\{\mathbf{t}_j \in \mathbb{R}^2, j = 1, 2, \ldots, N\}$, generally one has to find a transformation $\mathbf{F} : \mathbb{R}^\mathbf{2} \to \mathbb{R}^\mathbf{2}$ that satisfies the following constraint

$$\mathbf{F}(\mathbf{x}_j) = \mathbf{t}_j. \tag{1}$$

The transformation with landmarks based on RBFs has the following form

$$\mathbf{F}(\mathbf{x}) = \mathbf{x} + \sum_{j=1}^{N} \boldsymbol{\alpha}_j \boldsymbol{\Phi}(\| \mathbf{x} - \mathbf{x}_j \|),$$

where $\boldsymbol{\Phi}$ is a RBF, $\alpha_j = (\alpha_{j1}, \alpha_{j2})$, and $\| \cdot \|$ denotes the Euclidean norm. Generally, each coordinate of the transformation is calculated separately, therefore the transformation can be described as $F_k(\mathbf{x}) = \mathbf{x} + \sum_{j=1}^{N} \alpha_{jk} \boldsymbol{\Phi}(\| \mathbf{x} - \mathbf{x}_j \|)$, $k = 1, 2$. The coefficients α_{jk} have to be computed, and the unique solvability is a necessary condition to be satisfied. However, we know that $F_k(\mathbf{x}_j) = \mathbf{t}_{kj}$ has a unique solution if the function $\boldsymbol{\Phi}$ is strictly positive definite on $\mathbb{R}^2$ (see e.g. [7, 36, 13]).

CSRBFs and globally supported RBFs have their own benefits for image registration. CSRBFs can guarantee the locality of deformation, whereas small bending energy can be obtained by globally supported RBFs. In the following we will use some of the most popular compactly supported Gneiting functions and globally supported Matérn ones as transformation formulas.

2.1. Gneiting's functions

Starting with Wendland functions and applying the turning bands operator, Gneiting obtained a family of compactly supported functions [17]. Following [13], we can start with a function ψ_s that is strictly positive definite and radial on $\mathbb{R}^s$ for $s \geq 3$, and applying the turning bands operator results

$$\psi_{s-2}(r) = \psi_s(r) + \frac{r\psi_s'(r)}{s-2}, \tag{2}$$

which is strictly positive definite and radial on $\mathbb{R}^{s-2}$. For example, starting with the Wendland function $\psi_{4,1}(r) = (1-r)_+^{l+1}$ $[(l+1)r+1]$ and applying the turning bands operator we obtain the functions

$$\tau_{2,l}(r) = (1-r)_+^l \left(1 + lr - \frac{(l+1)(l+4)}{2} r^2\right), \tag{3}$$

which are strictly positive definite and radial on $\mathbb{R}^2$ provided $l \geq 7/2$. We list some specific $C^2(\mathbb{R})$ functions from this family for two choices of l, i.e.,

$$\tau_{2,7/2}(r) \doteq \left(1 - \frac{r}{c}\right)_+^{7/2} \left(1 + \frac{7}{2}\frac{r}{c} - \frac{135}{8}\left(\frac{r}{c}\right)^2\right), \tag{4}$$

and

$$\tau_{2,5}(r) \doteq \left(1 - \frac{r}{c}\right)_+^{5} \left(1 + 5\frac{r}{c} - 27\left(\frac{r}{c}\right)^2\right), \tag{5}$$

where c is the shape parameter used to define the width or the support size of transformations and $(\cdot)_+$ is the truncated power function. We evaluate the performances of Gneiting functions in image registration and compare the image registration properties with $\psi_{3,1} = (1 - \frac{r}{c})_+^4(4\frac{r}{c} + 1)$. Such function is strictly positive definite in $\mathbb{R}^s$, for $s \leq 3$, and commonly used in approximation problems.

2.2. Matérn functions

Matérn functions are quite common in the statistics literature and they have recently received a great deal of attention. The following formula is the general form of Matérn functions [18],

$$M(r \mid v) = \frac{2^{1-v}}{\Gamma(v)} r^v K_v(r), \tag{6}$$

where K_v is the *Modified Bessel Function of the second kind of order v.* The Fourier transform of the Matérn functions is given by the *Bessel kernels*

$$\hat{M}(w) = \left(1 + w^2\right)^{-\beta} > 0,$$

where $\beta = v + \frac{s}{2}$, and s is the dimension of the space, here $s = 2$. From the above Fourier transform, Matérn functions are strictly positive definite and radial on $\mathbb{R}^s$ for all $s < 2\beta$, which guarantees the unique solvability of coefficients. The three specific Matérn functions we consider here are

$$M_{1/2} = M\left(r \mid \frac{1}{2}, c\right) = \frac{2^{\frac{1}{2}}}{\Gamma(\frac{1}{2})}\left(\frac{r}{c}\right)^{\frac{1}{2}} K_{\frac{1}{2}}\left(\frac{r}{c}\right) \doteq e^{-r/c},$$

$$M_{3/2} = M\left(r \mid \frac{3}{2}, c\right) = \frac{2^{-\frac{1}{2}}}{\Gamma(\frac{3}{2})}\left(\frac{r}{c}\right)^{\frac{3}{2}} K_{\frac{3}{2}}\left(\frac{r}{c}\right) \doteq \left(1 + \frac{r}{c}\right)e^{-r/c},$$

$$M_{5/2} = M\left(r \mid \frac{5}{2}, c\right) = \frac{2^{-\frac{3}{2}}}{\Gamma(\frac{5}{2})}\left(\frac{r}{c}\right)^{\frac{5}{2}} K_{\frac{5}{2}}\left(\frac{r}{c}\right) \doteq \left(1 + \frac{r}{c} + \frac{1}{3}\frac{r^2}{c^2}\right)e^{-r/c},$$

where c has the same meaning as a parameter of Gneiting functions mentioned in Subsection 2.1.

3. Topology preservation in one-landmark matching

Topology preservation is a necessary requirement for image registration. To preserve topology, the necessary condition is the continuity of the function Φ and the positivity of the determinant of Jacobian matrix generated by $\mathbf{F}$ at each point. In this section, we briefly recall some results contained in [5, 10]. We consider the situation of one landmark matching where the source landmark $\mathbf{p}$ is shifted by Δ_x along the x-axis direction and by Δ_y along the y-axis direction to the target landmark $\mathbf{q}$. The coordinates of the transformation are

$$\begin{aligned} F_1(\mathbf{x}) &= x + \Delta_x \Phi(\|\mathbf{x} - \mathbf{p}\|), \\ F_2(\mathbf{x}) &= y + \Delta_y \Phi(\|\mathbf{x} - \mathbf{p}\|), \end{aligned} \tag{7}$$

where Φ is any RBF. From [16] we know that in 2D case the condition to keep positivity of the determinant is

$$\Delta \frac{\partial \Phi}{\partial r} > -\frac{1}{\sqrt{2}} \tag{8}$$

with $\Delta = \max(\Delta x, \Delta y)$ and $r = \|\mathbf{x} - \mathbf{p}\|$. This shows that the transformations defined by different RBFs preserve topology if inequality (8) holds. As mentioned in Section 1 the support size of RBFs can determine the width of registration. Precisely, the larger support size is, the larger deformation field is and vice versa. Therefore, if we could find the minimum value of support size under the condition (8), the deformation field would be the smallest in which topology preservation occurs. In particular, the smallest support size satisfying the constraint (8) is called optimal locality parameter. In next subsections, we will compare the optimal locality parameters of $\psi_{3,1}$, $\tau_{2,7/2}$, $\tau_{2,5}$, $M_{1/2}$, $M_{3/2}$ and $M_{5/2}$.

The optimal locality parameters of different transformations depend on $(\frac{\partial \Phi}{\partial r})_{min}$. Through calculations, we get the results showed in Table 1. As we mentioned before, small locality parameter means the influence area at each landmark is small. In fact this is beneficial for local deformation of images. For each isolated landmark, these conditions are valid only if no other landmark is placed within the radius. For landmarks with overlapping support area, calculation of optimal locality parameter is quite complex. In Section 5, we will study the behaviour of these transformations in this case. But in one landmark matching, if the distance among landmarks is large, the landmarks space is sparse. For this reason, we say that having a smaller optimal locality parameter is better. Table 1 shows that the first three CSRBFs, i.e. $\psi_{3,1}$, $\tau_{2,7/2}$ and $\tau_{2,5}$, have optimal parameters larger than the three Matérn functions considered. Hence, in this point, $M_{5/2}$ performs very well and $M_{1/2}$, $M_{3/2}$ are better than CSRBFs. Nevertheless, $\psi_{3,1}$ is better than $\tau_{2,7/2}$ and $\tau_{2,5}$ because the optimal locality parameter is smaller.

$\psi_{3,1}$	$\tau_{2,7/2}$	$\tau_{2,5}$	$M_{1/2}$	$M_{3/2}$	$M_{5/2}$
$c > 2.98\Delta$	$c > 5.09\Delta$	$c > 6.26\Delta$	$c > 1.10\Delta$	$c > 0.52\Delta$	$c > 0.3960\Delta$

Table 1: Optimal locality parameters of different RBFs.

Some numerical results about topology preservation in this case can be found in [5, 10]. We observe that if locality parameter c is much smaller than the optimal one, the deformed image will deeply be misrepresented above all around the shifted point. Conversely, if the parameter is very large, the image will be deformed in the whole field.

4. Topology preservation for limited deformations: theoretical and numerical study

The computation of the optimal support value is much more complicated when several landmarks influence the same region. For simplicity, we first consider the case of two single landmarks [37].

Let $P = \{(0, 0), (d, l)\}$ be two landmarks in the source image and suppose that they are sent in $Q = \{(0, \Delta), (d, l-\Delta)\}$ in the target image, where d and l denote the horizontal and vertical distances between the two landmarks of the source image, whereas Δ is the displacement along vertical direction. To simplify the comparison we assume that the displacement for both landmarks is the same, i.e. Δ, but in opposite direction. In this model, when either the two landmarks are very close, or the distance is very large, the topology might be difficult to preserve after deformation.

In this case, the locality parameter c is chosen large enough to ensure the influence regions of the two landmarks intersect each other. On the other hand, small locality parameters result in a non-preserving topology similar to the one-landmark matching case. Moreover, we assume $\Delta < \max(d, l)$ to guarantee existence of the optimal locality parameter, essential condition to have the topology preservation.

Let us now consider components of a generic transformation $\mathbf{F} : \mathbb{R}^2 \to \mathbb{R}^2$ obtained by a transformation of two points, i.e.,

$$F_1(\mathbf{x}) = x + \alpha_{1,1}\Phi(\|\mathbf{x} - P_1\|) + \alpha_{1,2}\Phi(\|\mathbf{x} - P_2\|),$$

and

$$F_2(\mathbf{x}) = y + \alpha_{2,1}\Phi(\|\mathbf{x} - P_1\|) + \alpha_{2,2}\Phi(\|\mathbf{x} - P_2\|).$$

We acquire coefficients $\alpha_{1,1}$, $\alpha_{1,2}$, $\alpha_{2,1}$ and $\alpha_{2,2}$ so that the transformation transmits points P_1 and P_2 in Q_1 and Q_2, respectively. To do that, we require that

$$F_1((0,0)) = 0, \qquad F_1((d,l)) = d$$

and

$$F_2((0,0)) = \Delta, \qquad F_2((d,l)) = l - \Delta.$$

Solving these two systems of two equations in two unknowns, we get

$$\alpha_{1,1} = 0, \;\; \alpha_{1,2} = 0, \;\; \alpha_{2,1} = \frac{\Delta}{1 - \Phi\left(\sqrt{d^2 + l^2}\right)}, \;\; \alpha_{2,2} = -\alpha_{2,1}.$$

It follows that the determinant of the Jacobian matrix is

$$\det\left(J(x,y)\right) = 1 + \alpha_{2,1}\frac{\partial\Phi\left(\sqrt{x^2+y^2}/c\right)}{\partial y} + \alpha_{2,2}\frac{\partial\Phi\left(\sqrt{(x-d)^2+(y-l)^2}/c\right)}{\partial y}, \tag{9}$$

and its minimum value is occurred at the midpoint between P_1 and P_2, i.e., $\left(\frac{d}{2}, \frac{l}{2}\right)$, when $\Delta > 0$ and the intersection of the influence regions of two landmarks does not turn out to be negligible. We thus obtain the optimal locality parameter when

$$\det\left(J\left(\frac{d}{2}, \frac{l}{2}\right)\right) = 0. \tag{10}$$

Obviously, one can observe that

$$\left.\frac{\partial\Phi\left(\sqrt{x^2+y^2}/c\right)}{\partial y}\right|_{x=\frac{d}{2}, y=\frac{l}{2}} = -\left.\frac{\partial\Phi\left(\sqrt{(x-d)^2+(y-l)^2}/c\right)}{\partial y}\right|_{x=\frac{d}{2}, y=\frac{l}{2}},$$

so we get

$$\det\left(J\left(\frac{d}{2}, \frac{l}{2}\right)\right) = 1 + 2\alpha_{2,1}\left.\frac{\partial\Phi\left(\sqrt{x^2+y^2}/c\right)}{\partial y}\right|_{x=\frac{d}{2}, y=\frac{l}{2}}. \tag{11}$$

4.1. Gneiting $\tau_{2,7/2}$

To find the optimal value of the parameter c, using Gneiting function $\tau_{2,7/2}$, we obtain (11) and compute the value of $\alpha_{2,1}$, i.e.,

$$\alpha_{2,1} = \frac{\Delta}{1 - \left(1 - \frac{\sqrt{d^2+l^2}}{c}\right)^{7/2}\left(1 + \frac{7}{2}\frac{\sqrt{d^2+l^2}}{c} - \frac{135}{8}\frac{d^2+l^2}{c^2}\right)}.$$

Setting $r = \sqrt{x^2 + y^2}$, we evaluate (4) at $x = \frac{d}{2}$ and $y = \frac{l}{2}$

$$\left.\frac{\partial\Phi\left(\sqrt{x^2+y^2}/c\right)}{\partial y}\right|_{x=\frac{d}{2}, y=\frac{l}{2}} = -\frac{99}{32}\frac{l}{c^2}\left(1-\frac{\sqrt{d^2+l^2}}{2c}\right)^{5/2}\left(8-15\frac{\sqrt{d^2+l^2}}{2c}\right). \tag{12}$$

Substituting then (12) in (11), we obtain

$$\det\left(J\left(\frac{d}{2},\frac{l}{2}\right)\right) = 1 - \frac{99}{16c^2}\frac{\Delta l\left(1-\frac{\sqrt{d^2+l^2}}{2c}\right)^{5/2}\left(8-15\frac{\sqrt{d^2+l^2}}{2c}\right)}{1-\left(1-\frac{\sqrt{d^2+l^2}}{c}\right)^{7/2}\left(1+\frac{7}{2}\frac{\sqrt{d^2+l^2}}{c}-\frac{135}{8}\frac{d^2+l^2}{c^2}\right)}. \tag{13}$$

From (10) it follows that the optimal parameter c for the Gneiting function $\tau_{2,7/2}$ is the solution of the equation (13), providing

$$\frac{d^2+l^2}{c^2} < 1.$$

4.2. Gneiting $\tau_{2,5}$

We look for the optimal value of the parameter c, using Gneiting function $\tau_{2,5}$. Then we compute $\alpha_{2,1}$, obtaining

$$\alpha_{2,1} = \frac{\Delta}{42\frac{z}{c^2} - 175\frac{z^{3/2}}{c^3} + 315\frac{z^2}{c^4} - 294\frac{z^{5/2}}{c^5} + 140\frac{z^3}{c^6} - 27\frac{z^{7/2}}{c^7}},$$

where, to simplify notation, we set $z = d^2 + l^2$.

Evaluating (5) at $x = \frac{d}{2}$ and $y = \frac{l}{2}$, we derive

$$\begin{aligned}\left.\frac{\partial\Phi\left(\sqrt{x^2+y^2}/c\right)}{\partial y}\right|_{x=\frac{d}{2}, y=\frac{l}{2}} &= -\frac{21}{2}\frac{l}{c^2}\left(4-\frac{7}{2}\frac{(d^2+l^2)^{1/2}}{c}-3\frac{d^2+l^2}{c^2}\right.\\ &\left.+\frac{19}{4}\frac{(d^2+l^2)^{3/2}}{c^3}-2\frac{(d^2+l^2)^2}{c^4}+\frac{9}{2}\frac{(d^2+l^2)^{5/2}}{c^5}\right).\end{aligned} \tag{14}$$

Replacing now (14) in (11), we get

$$\det\left(J\left(\frac{d}{2},\frac{l}{2}\right)\right) = 1 - \frac{21\Delta l\left(4-\frac{7}{2}\frac{z^{1/2}}{c}-3\frac{z}{c^2}+\frac{19}{4}\frac{z^{3/2}}{c^3}-2\frac{z^2}{c^4}+\frac{9}{2}\frac{z^{5/2}}{c^5}\right)}{42z - 175\frac{z^{3/2}}{c} + 315\frac{z^2}{c^2} - 294\frac{z^{5/2}}{c^3} + 140\frac{z^3}{c^4} - 27\frac{z^{7/2}}{c^5}}. \tag{15}$$

From (10) we deduce that the optimal parameter c for the Gneiting function $\tau_{2,5}$ is obtained by finding the solution of the equation (15), provided that

$$\frac{d^2+l^2}{c^2} < 1.$$

4.3. Matérn $M_{1/2}$

From (7), the optimal locality parameter c can be derived as

$$\alpha_{2,1} = \frac{\Delta}{1 - e^{-\sqrt{d^2+l^2}/c}},$$

and

$$\left.\frac{\partial\Phi\left(\sqrt{x^2+y^2}/c\right)}{\partial y}\right|_{x=\frac{d}{2},y=\frac{l}{2}} = -\frac{l}{c\sqrt{d^2+l^2}}e^{-\frac{\sqrt{d^2+l^2}}{2c}}. \tag{16}$$

According to (11), the determinant of Jacobian matrix generated by $M_{1/2}$ is given by

$$\det\left(J\left(\frac{d}{2},\frac{l}{2}\right)\right) = 1 - \frac{2l\Delta e^{-\sqrt{d^2+l^2}/2c}}{c\sqrt{d^2+l^2}\left(1-e^{-\sqrt{d^2+l^2}/c}\right)}. \tag{17}$$

4.4. Matérn $M_{3/2}$

Similarly, according to (7) the determinant of its Jacobian matrix can be calculated as follows

$$\alpha_{2,1} = \frac{\Delta}{1-\left(1+\frac{\sqrt{d^2+l^2}}{c}\right)e^{-\sqrt{d^2+l^2}/c}},$$

and

$$\left.\frac{\partial\Phi\left(\sqrt{x^2+y^2}/c\right)}{\partial y}\right|_{x=\frac{d}{2},y=\frac{l}{2}} = -\frac{l}{2c^2}e^{-\frac{\sqrt{d^2+l^2}}{2c}}. \tag{18}$$

Now we obtain the Jacobian determinant of $M_{3/2}$, i.e.,

$$\det\left(J\left(\frac{d}{2},\frac{l}{2}\right)\right) = 1 - \frac{l\Delta e^{-\sqrt{d^2+l^2}/2c}}{c^2\left(1-\left(1+\frac{\sqrt{d^2+l^2}}{c}\right)\right)e^{-\sqrt{d^2+l^2}/c}}. \tag{19}$$

4.5. Matérn $M_{5/2}$

Considering the same process of calculation used in the previous subsections, the determinant of Jacobian matrix of (7) can be described as

$$\alpha_{2,1} = \frac{\Delta}{1-\left(1+\frac{\sqrt{d^2+l^2}}{c}+\frac{d^2+l^2}{3c^2}\right)e^{-\sqrt{d^2+l^2}/c}},$$

and

$$\left.\frac{\partial\Phi\left(\sqrt{x^2+y^2}/c\right)}{\partial y}\right|_{x=\frac{d}{2},y=\frac{l}{2}} = -\frac{l}{6c^2}\left(1+\frac{\sqrt{d^2+l^2}}{2c}\right)e^{-\frac{\sqrt{d^2+l^2}}{2c}}. \tag{20}$$

Based on (11), we can get the determinant of $M_{5/2}$ Jacobian matrix as follows

$$\det\left(J\left(\frac{d}{2},\frac{l}{2}\right)\right) = 1 - \frac{l\Delta e^{-\sqrt{d^2+l^2}/2c}\left(1+\frac{\sqrt{d^2+l^2}}{2c}\right)}{3c^2\left(1-\left(1+\frac{\sqrt{d^2+l^2}}{c}+\frac{d^2+l^2}{3c^2}\right)e^{-\sqrt{d^2+l^2}/c}\right)}. \tag{21}$$

4.6. Analysis

Figure 1 shows the behaviour of the optimal locality parameter c by varying Δ, for d and l fixed. In both cases we may note that function $\tau_{2,5}$ needs much larger supports to preserve the topology property than other RBFs that we evaluated. With Δ larger, the value of support size of $\tau_{2,5}$ increases significantly, especially in the first case when $d = l = 32$. The functions $\psi_{3,1}$ and $\tau_{2,7/2}$ have very similar behaviour. In fact, the latter have relative smaller optimal support size, whereas Matérn functions need much smaller supports than these CSRBFs. For instance, when $\Delta = 29$, for $M_{1/2}$ and $M_{3/2}$, c is less than 100 and for $M_{5/2}$ c is less than 50. For other functions, c is more than 100 and less than 150, exception for $\tau_{2,5}$ whose value of c is larger than 1000. We obtain the same result as Figure 6 shows us.

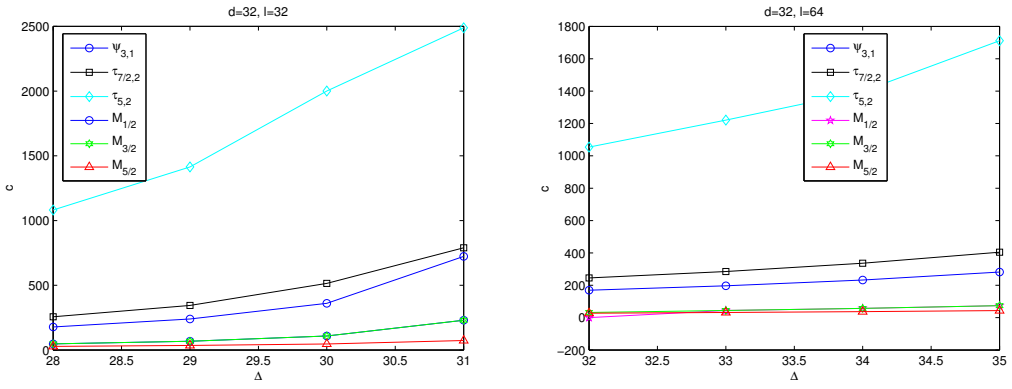

(a) (b)

Figure 1: In (a), we show the optimal locality parameter c in the two-landmark matching case by varying Δ with $d = l = 32$, while in (b) those with $d = 32$ and $l = 64$.

Let us now consider a uniform grid 257×257 whose deformation is given by the displacement of two landmarks. By varying the displacement of such points, we can compare results by two criteria [37]:

1. *The number of points where the determinant of the Jacobian is negative.* Such number indicates the size of the region with violated topology preservation.
2. *The average of the negative Jacobian determinants.* This parameter represents the severity of topology violation. So the more the value is negative, the more the transformation might be bent or broken compared to the original structure.

Figures 2-5 point out the point number where the determinant is negative and the average of negative determinants, both of them computed by varying values of c. In particular, Figure 2 represents the matching case of very large deformation ($d = l = 32$, $\Delta = 28$). When c is small, for example $c = 45$, except for $M_{5/2}$, all other functions result in severe topology violations. $M_{1/2}$ and $M_{3/2}$ have a smaller number of points in which $\det(J(x, y)) < 0$ than $\psi_{3,1}$, $\tau_{2,7/2}$ and $\tau_{2,5}$. This means the violation fields of $M_{1/2}$ and $M_{3/2}$ are smaller. On the contrary, $\psi_{3,1}$ presents the largest number of points in which $\det(J(x, y)) < 0$ and a relatively larger average in modulus. Moreover, this graph shows that $\psi_{3,1}$ violates the topology preservation in the largest areas, and its violations turn out to be relatively slight compared with $\tau_{2,7/2}$ and $\tau_{2,5}$. Among the considered CSRBFs, $\tau_{2,5}$ violates the smallest area, but it presents a small mean value in modulus and therefore we have a more significant topology violation in a slightly smaller region. When c is large, such as $c = 120$, $M_{3/2}$ and $M_{5/2}$ can preserve topology well, since the number of points in $\det(J(x, y)) < 0$ is almost equal to zero, so there is almost no field violation. We can observe that, when c is larger, the negative number of points of $\det(J(x, y))$ of $\psi_{3,1}$ is smaller and, when $c = 120$, it has a negative number points smaller than $\tau_{2,7/2}$ and $\tau_{2,5}$. A diametrically opposite situation happens when $c = 45$. In this case, $\psi_{3,1}$ has a larger violation area.

Figure 3 depicts the case of a relatively large deformation ($d = 32$, $l = 64$, $\Delta = 32$). For small supports, such as $c = 60$, all Matérn functions preserve topology, whereas the CSRBFs $\psi_{3,1}$, $\tau_{2,7/2}$ and $\tau_{2,5}$ have violation areas. Among them, $\tau_{2,7/2}$ and $\tau_{2,5}$ do not preserve the topology of a small region, oppositely $\psi_{3,1}$ has much smaller violation area.

Furthermore, by increasing support we have a more extended topology non-preservation using $\tau_{2,7/2}$ and $\tau_{2,5}$, whereas for other functions we have a progressive improvement, up to obtain much small regions in the case of $\psi_{3,1}$.

Finally, Figures 4-5 refer to the case of $\Delta < 0$. When $d = 8$, $l = 0$ and $\Delta = -8$ there is no topology violation for the RBFs we considered. Instead, if $\Delta = -16$, a quite different situation occurs. $M_{5/2}$ has a very large number of negative points of $\det(J(x, y))$ and, increasing the number of support size, the violation region increases significantly until $c = 130$. This means that in this case $M_{5/2}$ violate image in very large regions, but we can see that it is stable and has relative large average in modulus which means its violation turns out to be slight. All the other RBFs have relative small negative points. Among them, $M_{1/2}$ has the smallest average, therefore it has the most severe violations. Moreover, the functions $\tau_{2,7/2}$ and $\tau_{2,5}$ have more slight violation than $M_{1/2}$ but more severe than $\psi_{3,1}$.

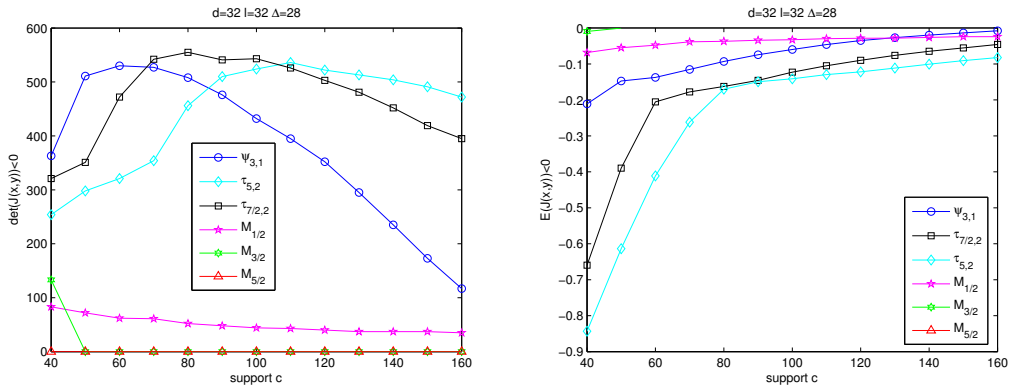

Figure 2: In the two-landmark case we show: the number of points where there is no topology preservation by varying the support with $d = 32$, $l = 32$ and $\Delta = 28$ in the left figure; the average of the negative Jacobian determinants by varying the support with $d = 32$, $l = 32$ and $\Delta = 28$ in the right figure.

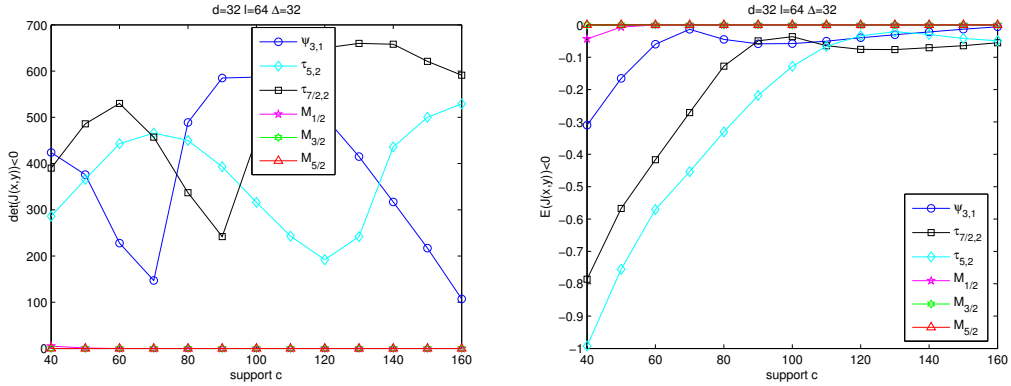

Figure 3: In the two-landmark case we show: the number of points where there is no topology preservation by varying the support with $d = 32$, $l = 64$ and $\Delta = 32$ in the left figure; the negative Jacobian determinants by varying the support with $d = 32$, $l = 64$ and $\Delta = 32$ in the right figure.

4.7. Numerical results

We consider a grid $[0, 1] \times [0, 1]$ and then compare results obtained by the grid distortion in the shift case of two landmarks $\{(0.375, 0.350), (0.625, 0.55)\}$ in $\{(0.375, 0.5), (0.625, 0.4)\}$, respectively. We report Figure 6 using $c = 0.5$

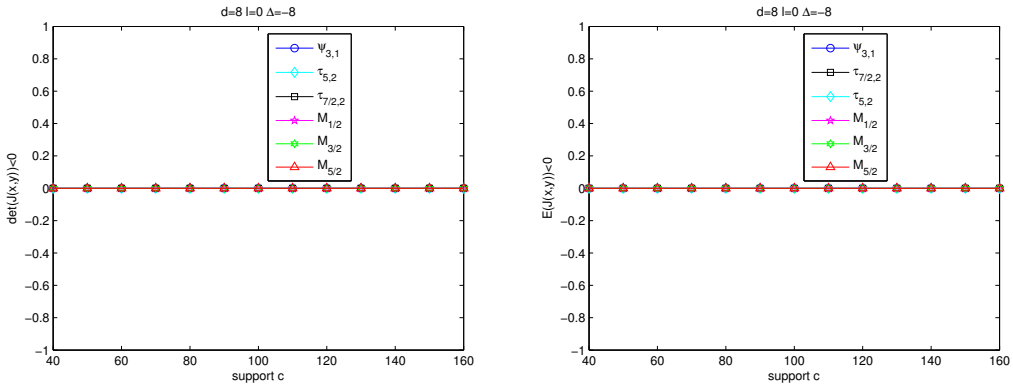

Figure 4: In the two-landmark case we show: the number of points where there is no topology preservation by varying the support with $d = 8$, $l = 0$ and $\Delta = -8$ in the left figure; the average of the negative Jacobian determinants by varying the support with $d = 8$, $l = 0$ and $\Delta = -8$ in the right figure.

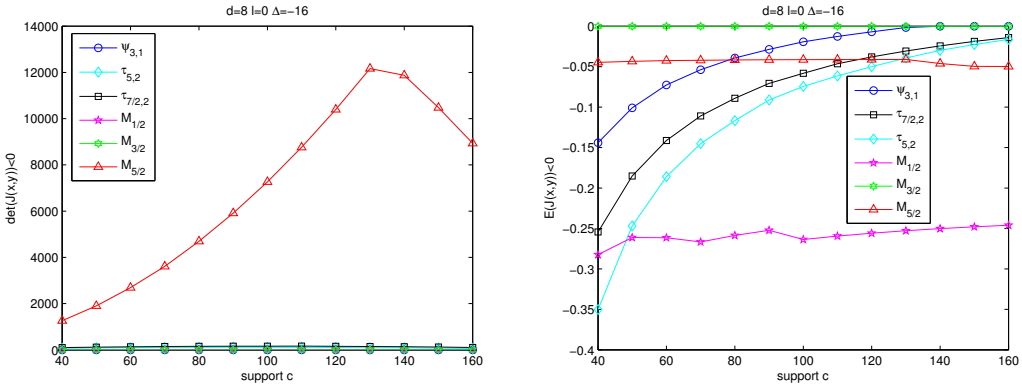

Figure 5: In the two-landmark case we show: the number of points where there is no topology preservation by varying the support with $d = 8$, $l = 0$ e $\Delta = -16$ in the left figure; the average of the negative Jacobian determinants by varying the support with $d = 8$, $l = 0$ and $\Delta = -16$ in the right figure.

as support size for CSRBFs and relative small shape parameters for Matérn functions. In fact, they are $c = 0.1$ for $M_{3/2}$ and $M_{5/2}$. We observe that Gneiting functions present, unlike other functions, a good topology preservation in the areas where there is no any influence of the modified landmarks, but a severe distortion in the region of landmarks' influence. This outcome is in agreement with the results obtained in the previous section where from Figure 2 we noted that Gneiting functions present a smaller number of points having a negative Jacobian determinant, but at these points the average turns out to be a negative number smaller than that of other functions. Oppositely, Matérn functions can preserve topology well in the region and slight distortion of landmark's influence, even if in this case the whole image is deformed slightly. When support size is relatively large, for instance $c = 0.5$, we can see the severe deformation of the whole image as the Figure 7 shows us.

5. Topology preservation for more extended deformations

In this section, we evaluate topology preservation of RBFs for four landmarks. We divide this section into two parts. In the first part, we discuss topology properties with very large supports such that they are able to cover the whole domain. In this case, the influence of each landmark extends on the entire image, thus generating global

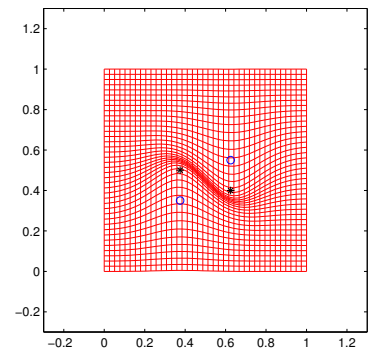

(a) Wendland $\psi_{3,1}$, $c = 0.5$

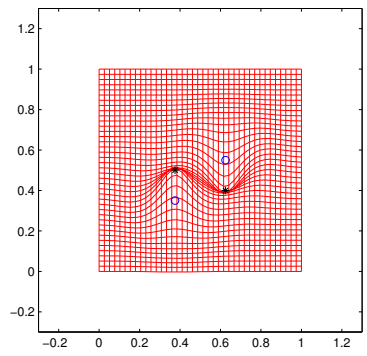

(b) Gneiting $\tau_{2,5}$, $c = 0.5$

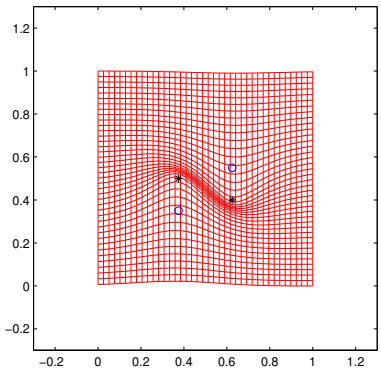

(c) Matérn $M_{3/2}$, $c = 0.1$

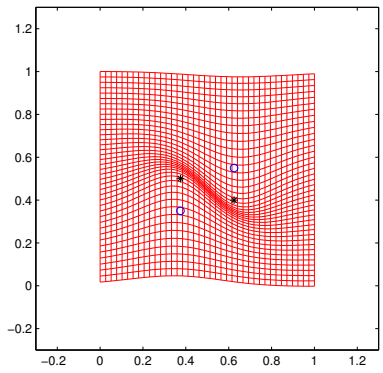

(d) Matérn $M_{5/2}$, $c = 0.1$

Figure 6: Deformation results of two-landmarks matching; the source landmarks are marked by a circle ($\circ$), while the target ones by a star ($*$).

deformations. For this aim, we consider four inner landmarks in a grid, located so as to form a rhombus at the center of the figure, and we suppose that only the lower vertex is downward shifted of Δ [37]. The landmarks of source and target images are $P = \{(0,1),(-1,0),(0,-1),(1,0)\}$ and $Q = \{(0,1),(-1,0),(0,-1-\Delta),(1,0)\}$, respectively, with $\Delta > 0$. In the second part, we study the specific case that the distance between two landmarks is very small. This means that the two deformed fields will be intersected, thus topology violation will occur. For analyzing the properties of RBFs in this situation, we analytically compare the results of numerical experiments among these RBFs.

5.1. Global deformation for four landmarks

Let us now consider components of a generic transformation $\mathbf{F} : \mathbb{R}^2 \to \mathbb{R}^2$ obtained by a transformation of four points P_1, P_2, P_3 and P_4, namely

$$F_1(\mathbf{x}) = x + \sum_{i=1}^{4} \alpha_{1,i} \Phi(\|\mathbf{x} - P_i\|),$$

$$F_2(\mathbf{x}) = y + \sum_{i=1}^{4} \alpha_{2,i} \Phi(\|\mathbf{x} - P_i\|).$$

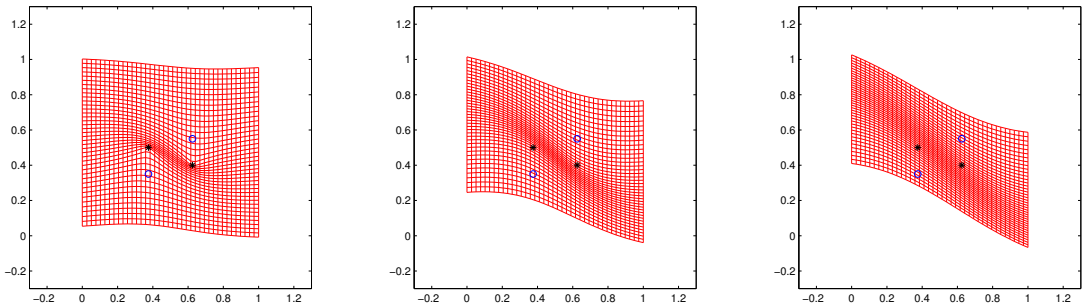

Figure 7: The whole deformation results of two-landmarks matching for Matérn functions $M_{1/2}$ (left), $M_{3/2}$ (center) and $M_{5/2}$ (right) with $c = 0.5$; the source landmarks are marked by a circle ($\circ$), while the target ones by a star ($*$).

The x-axis coefficients matrix is obtained as (22), so that the transformation sends P_i to Q_i, with $i = 1, \ldots, 4$,

$$\begin{pmatrix} 1 & \alpha & \beta & \alpha \\ \alpha & 1 & \alpha & \beta \\ \beta & \alpha & 1 & \alpha \\ \alpha & \beta & \alpha & 1 \end{pmatrix} \begin{pmatrix} \alpha_{1,1} \\ \alpha_{1,2} \\ \alpha_{1,3} \\ \alpha_{1,4} \end{pmatrix} = \begin{pmatrix} 0 \\ 0 \\ 0 \\ 0 \end{pmatrix} \tag{22}$$

and the y-axis coefficients matrix has the following form:

$$\begin{pmatrix} 1 & \alpha & \beta & \alpha \\ \alpha & 1 & \alpha & \beta \\ \beta & \alpha & 1 & \alpha \\ \alpha & \beta & \alpha & 1 \end{pmatrix} \begin{pmatrix} \alpha_{2,1} \\ \alpha_{2,2} \\ \alpha_{2,3} \\ \alpha_{2,4} \end{pmatrix} = \begin{pmatrix} 0 \\ 0 \\ -\Delta \\ 0 \end{pmatrix} \tag{23}$$

where $\alpha = \Phi\left(\frac{\sqrt{2}}{c}\right)$ and $\beta = \Phi\left(\frac{2}{c}\right)$. The solutions of the systems (22) and (23) are

$$\alpha_{1,1} = 0, \quad \alpha_{1,2} = 0, \quad \alpha_{1,3} = 0, \quad \alpha_{1,4} = 0, \tag{24}$$

and

$$\begin{aligned} \alpha_{2,1} &= \frac{\beta^2 + \beta - 2\alpha^2}{(1-\beta)[(1+\beta)^2 - 4\alpha^2]}\Delta, \quad \alpha_{2,2} = \frac{\alpha}{(1+\beta)^2 - 4\alpha^2}\Delta, \\ \alpha_{2,3} &= -\frac{1 + \beta - 2\alpha^2}{(1-\beta)[(1+\beta)^2 - 4\alpha^2]}\Delta, \quad \alpha_{2,4} = \alpha_{2,2}. \end{aligned} \tag{25}$$

For simplicity, we denote $\Phi_i = \Phi(\|(x, y) - P_i\|/c), i = 1, \ldots, 4$.

The determinant of the Jacobian matrix is

$$\det\left(J(x, y)\right) = 1 + \sum_{i=1}^{4} \alpha_{2,i} \frac{\partial \Phi_i}{\partial y}. \tag{26}$$

In this case, the influence of each landmark occurs on the whole image, hence the support c we choose is very large to fulfill this aim. Since computation of the Jacobian matrix determinant in four landmarks is complex, we use Taylor expansion and consider $\|\cdot\|/c$ to be infinitesimal so that omit terms of higher order to approximate functions.

For complexity of calculations, we use Taylor expansion and omit higher order terms to approximate RBFs which we evaluate in above sections. The process to calculate them is:

- `Step 1`: using Taylor expansion to approximate RBFs.

- `Step 2`: calculating α and β so that coefficients can be obtained using the approximations in `Step 1`. In this step, through calculation we obtain the approximations

$$\alpha_{2,1} \approx -\alpha_{2,2} \approx \alpha_{2,3} \approx -\alpha_{2,4}.$$

In fact, for example, being $\beta \approx 2\alpha - 1$, we have

$$\begin{aligned}\alpha_{2,1} &\approx \frac{\beta^2+\beta-2\alpha^2}{(1-\beta)[(1+\beta)^2-4\alpha^2]}\Delta \\ &\approx \frac{4\alpha^2-4\alpha+1+2\alpha-1-2\alpha^2}{(1-2\alpha+1)[(1+\beta)^2-4\alpha^2]}\Delta \\ &= -\frac{2\alpha(1-\alpha)}{2(1-\alpha)[(1+\beta)^2-4\alpha^2]}\Delta \\ &= -\frac{\alpha}{(1+\beta)^2-4\alpha^2}\Delta = -\alpha_{2,2}.\end{aligned}$$

- `Step 3`: using the approximation in `Step 1` to approximate the first derivatives of different RBFs, then computing $\frac{\partial \Phi_i}{\partial y}$.
- `Step 4`: calculating the determinants of different RBFs using formula (26).

Through the four stages, we get the following determinant of different Jacobian matrices:

$$\det\left(J(0,y)\right)_{\psi_{3,1}} = \det\left(J(0,y)\right)_{\tau_{2,7/2}} = \det\left(J(0,y)\right)_{\tau_{2,5}} \approx 1 - 0.6402\Delta\left(y^2+1-y\sqrt{y^2+1}\right), \tag{27}$$

$$\det\left(J(0,y)\right)_{M_{1/2}} \approx 1 - 2.4142\Delta\left(-1+\frac{y}{\sqrt{y^2+1}}\right), \tag{28}$$

$$\det\left(J(0,y)\right)_{M_{3/2}} \approx 1 - 1.7071\Delta\left(y^2+1-y\sqrt{y^2+1}\right), \tag{29}$$

$$\det\left(J(0,y)\right)_{M_{5/2}} \approx 1 - 2.5607\Delta\left(y^2+1-y\sqrt{y^2+1}\right). \tag{30}$$

Further details on numerical experiments and some explanations on this studied case, where only one landmark is moved, can be found in [37, 10, 5].

5.2. Analysis of the locality parameter

In this part, we discuss the influence of locality parameter when distances among landmarks are small. To analytically compare the numerical results, the source landmarks we choose are $\{(0.5, 0.65), (0.35, 0.5), (0.65, 0.5), (0.5, 0.35)\}$ and the target ones are $\{(0.5, 0.65), (0.45, 0.5), (0.55, 0.5), (0.5, 0.35)\}$. Deformation occurs in x-axis direction. We note that the distance between two horizontal landmarks is only 0.3. The landmarks are very close and when deformation occurs in horizontal direction, violation occurs very easily. In previous sections, we evaluated optimal locality parameter to preserve topology after deformation using different RBFs. But in this case, the optimal locality parameter not only depends on the transformed functions but also depends on the position of the landmarks. The locality parameter we choose can not be larger than the deformed radius between the two landmarks: 0.15, otherwise, the two deformed field could be intersect.

Figure 8 shows the results when $c = 0.1$, which is smaller than the radius, and $c = 0.5$. We can observe that $\tau_{2,5}$ for $c = 0.1$ has much severe violation. This means that, in order to preserve topology, c has to be larger than 0.1. We observe that the intersection field of $\psi_{3,1}$ is smaller than $\tau_{2,5}$ when $c = 0.5$. $M_{3/2}$ has larger intersection field than any other RBF. This happens because they do not have compact support and deformation of each landmark affects the whole image. When $c = 0.1$, $M_{1/2}$ has a good performance: in fact, it can preserve topology well without intersecting deformation.

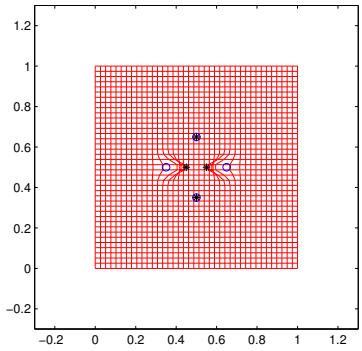

(a) Wendland $\psi_{3,1}$, $c = 0.1$

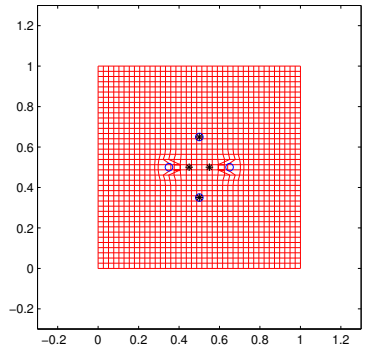

(b) Gneiting $\tau_{2,5}$, $c = 0.1$

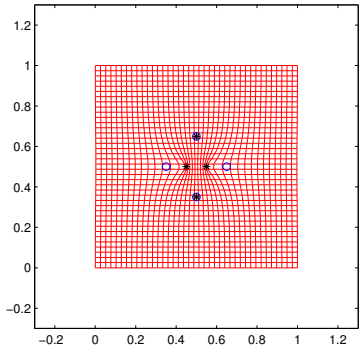

(c) Matérn $M_{1/2}$, $c = 0.1$

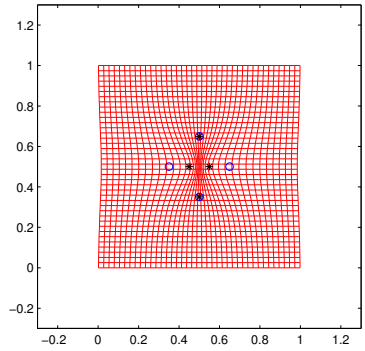

(d) Matérn $M_{3/2}$, $c = 0.1$

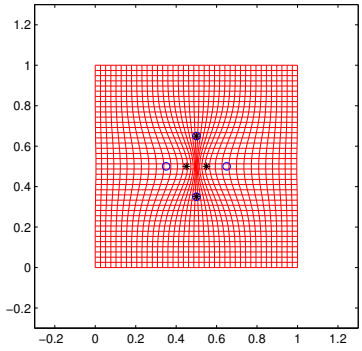

(e) Wendland $\psi_{3,1}$, $c = 0.5$

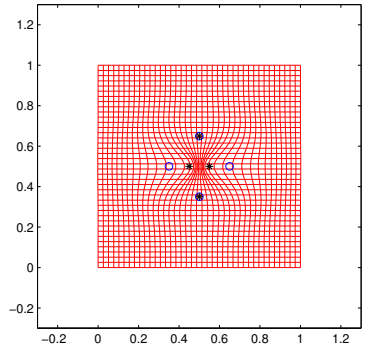

(f) Gneiting $\tau_{2,5}$, $c = 0.5$

Figure 8: Deformation results of four landmarks; the source landmarks are marked by a circle ($\circ$), while the target ones by a star ($*$).

6. Experimental results for simple objects using a large number of landmarks

In this section, we consider two pairs of schematic models for simple objects. They are square shift and scaling, which are discussed in [2], and circle contraction and expansion, which are evaluated in [22]; see also [3] for further test models. These experiments simulate classic medical cases, such as specific parts of images shift or scaling, either

shrink or grow.

6.1. Properties of various RBFs in square shift and scaling

Square shift and scaling of simple objects are considered in this subsection. We denote with $\mathcal{X}$ the set of 40×40 points of a regular grid superimposed on the source images. In shift case, we use 64 landmarks and 4 quasi-landmarks to transform the grid. In scaling model, we use 64 landmarks to evaluate the deformation of the various six transformations, which are considered in the above sections.

For analyzing the behaviour of these transformations in both of cases, we use the root mean square error (RMSE) as the test rule, which has the following form

$$\text{RMSE} = \sqrt{\frac{\sum_{\mathbf{x}\in\mathcal{X}} \| \mathbf{x} - \boldsymbol{F}(\mathbf{x}) \|_2^2}{\sum_{\mathbf{x}\in\mathcal{X}}}}. \tag{31}$$

In both of cases, the maximum displacement among landmarks is 0.1, therefore based on Table 1, we start with the optimal locality parameters of the six functions: 0.3, 0.509, 0.626, 0.11, 0.052 and 0.0396 to choose the smallest number of support size such that all the registration results are good as Figures 9 and 10 show us.

RBFs	RMSEs
$\psi_{3,1}$ $c = 0.4$	7.7628E-002
$\tau_{2,7/2}$ $c = 3.3$	8.7123E-002
$\tau_{2,5}$ $c = 1.1$	8.3158E-002
$M_{1/2}$ $c = 0.14$	8.2196E-002
$M_{3/2}$ $c = 0.083$	8.4720E-002
$M_{5/2}$ $c = 0.05$	7.8272E-002

RBFs	RMSEs
$\psi_{3,1}$ $c = 0.4$	6.5634E-002
$\tau_{2,7/2}$ $c = 0.9$	7.5910E-002
$\tau_{2,5}$ $c = 0.9$	6.7772E-002
$M_{1/2}$ $c = 0.14$	6.3797E-002
$M_{3/2}$ $c = 0.083$	7.0689E-002
$M_{5/2}$ $c = 0.067$	8.8005E-002

Table 2: Comparison of errors among different transformations in square shift (left) and square scaling (right).

In Table 2, we can observe that based on topology preservation condition, in shift case, $\psi_{3,1}$ and $M_{5/2}$ have very similar RMSEs which are smaller than the rest of RBFs. The other RBFs perform similar RMSEs with various c. Unlike $\psi_{3,1}$ and Matérn, Gneiting functions need much larger c to obtain good registration results in shift case. Moreover, we observe that the Wendland $\psi_{3,1}$ has a limited but larger deformation close to the shifted square, while in the rest of the image the result is smoother and not deformed. In square scaling, $M_{1/2}$ has the smallest RMSEs and relatively smaller c compared with the other RBFs. This means that it has a good similarity after registration. However, Figure 10 shows that $M_{1/2}$ achieves a smooth registration result. In this case, $\psi_{3,1}$, $\tau_{2,7/2}$ and $M_{3/2}$ give larger deformations and higher errors.

6.2. Properties of various RBFs in circle contraction and expansion

Other two test examples are circle contraction and expansion respectively. As already mentioned above, we still denote with $\mathcal{X}$ the set of 40×40 points of a regular grid superimposed on the source images. In both of cases, we use 20 source and target landmarks and 40 quasi-landmarks.

Similarly as the first two cases, when these functions are chosen to obtain good registration results with the smallest support size, the RMSEs are very similar (see Table 3). In view of the support size taken, we can see that in circle contraction $\tau_{2,7/2}$ needs a value of c much larger than other functions. Best results are obtained using the Matérn family. In particular, $M_{1/2}$ has small RMSEs in these schematic models with smooth registration results.

7. Real application to medical brain images

In this section, we evaluate registration results in two magnetic resonance brain images, which are displayed in Figure 13 (a)-(b). The pixels of the image is 256×256 and we choose 18 source landmarks marked by circle ($\circ$) and the corresponding 18 target landmarks marked by star ($*$). To acquire the results, we compare the images after registration obtained by using various RBFs. For brevity, we report only the most significant images. The results of

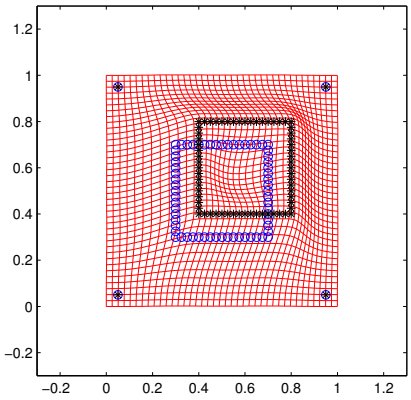

(a) Wendland $\psi_{3,1}$, $c = 0.4$

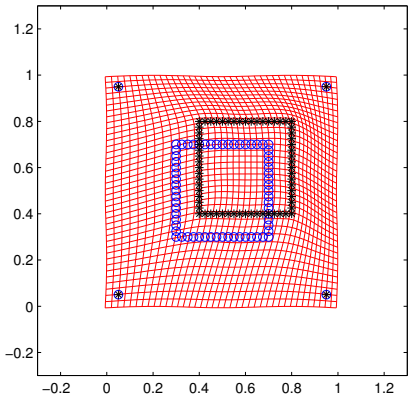

(b) Gneiting $\tau_{2,7/2}$, $c = 1.2$

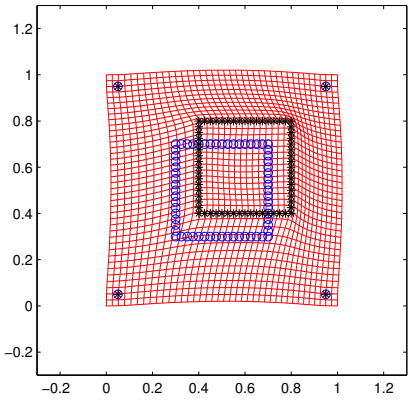

(c) Matérn $M_{1/2}$, $c = 0.14$

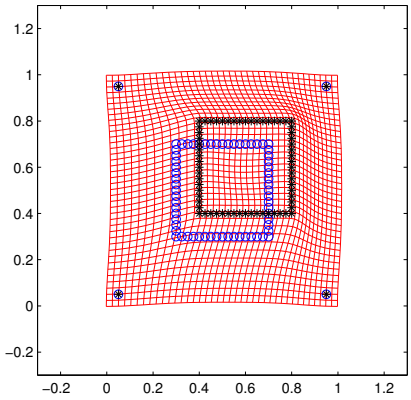

(d) Matérn $M_{3/2}$, $c = 0.083$

Figure 9: Deformation results of square shift; the source landmarks are marked by a circle ($\circ$), while the target ones by a star ($*$).

RBFs	RMSEs
$\psi_{3,1}$ $c = 0.4$	5.0239E-002
$\tau_{2,7/2}$ $c = 5$	5.3654E-002
$\tau_{2,5}$ $c = 0.7$	4.9016E-002
$M_{1/2}$ $c = 0.1$	4.0929E-002
$M_{3/2}$ $c = 0.083$	4.9917E-002
$M_{5/2}$ $c = 0.04$	4.4990E-002

RBFs	RMSEs
$\psi_{3,1}$ $c = 0.4$	3.8372E-002
$\tau_{2,7/2}$ $c = 0.55$	3.9521E-002
$\tau_{2,5}$ $c = 0.7$	3.6212E-002
$M_{1/2}$ $c = 0.1$	3.3222E-002
$M_{3/2}$ $c = 0.083$	3.9398E-002
$M_{5/2}$ $c = 0.04$	3.4984E-002

Table 3: Comparison of errors among different transformations in circle contraction (left) and circle expansion (right).

Figure 13 show that in this medical brain case, the shape parameter should be slightly larger than in test cases. We can observe that among these transformations, $M_{3/2}$ gives the best registration result; in particular, we remark that Matérn functions performs better with large shape parameters c and a relatively big number of landmarks. Good results are also obtained using the Gneiting family but they are not so good as Matérns are. This is probably due to the oscillating behaviour of Gneiting functions. Specifically, the best outcome is achieved by $\tau_{2,7/2}$ with $c = 5$. A very similar good

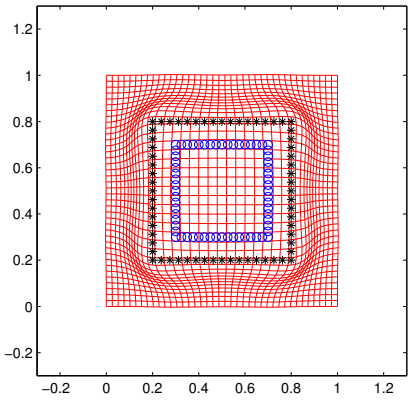

(a) Wendland $\psi_{3,1}$, $c = 0.4$

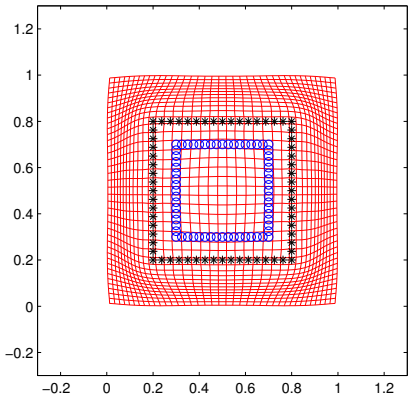

(b) Gneiting $\tau_{2,7/2}$, $c = 0.9$

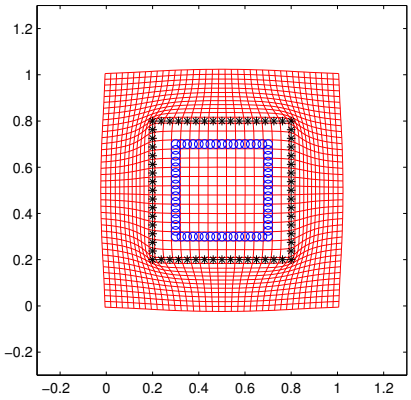

(c) Matérn $M_{1/2}$, $c = 0.14$

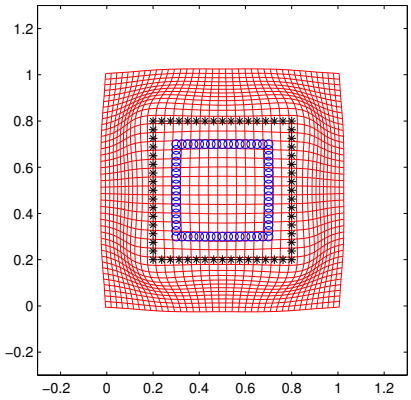

(d) Matérn $M_{5/2}$, $c = 0.067$

Figure 10: Deformation results of square scaling; the source landmarks are marked by a circle ($\circ$), while the target ones by a star ($*$).

performance for this function was previously obtained in the test case of circle contraction, see Table 3.

8. Conclusions

In this paper, we at first evaluated the performances of topology preservation for $\psi_{3,1}$, $\tau_{2,7/2}$, $\tau_{2,5}$, $M_{1/2}$, $M_{3/2}$ and $M_{5/2}$ in one, two and four landmarks. For the isolated landmark model, Matérn functions have the smallest optimal locality parameter. In particular, if no other landmark is placed within the radius, $M_{5/2}$ has the best performance among these RBFs. In two landmarks matching, with fixed landmarks, the number of optimal locality parameter c of Gneiting functions increases significantly when the displacements increase. On the other hand, Matérn functions need smaller optimal locality parameters. Generally, Matérn functions in this case violate images in smaller regions and their violations are slighter if we refer to the two criteria defined in Subsection 4.6. Conversely, Gneiting functions have much smaller averages when locality parameter is small, therefore Gneiting functions violate topology severely. When displacement is large with the opposite direction, we found numerical results for the Matérn family are better than the ones obtained with the other RBFs. More precisely, $M_{1/2}$ achieves better accuracy than $M_{3/2}$ and $M_{5/2}$. However, in general, except $M_{5/2}$, all the other RBFs we evaluated can preserve topology well because the number of

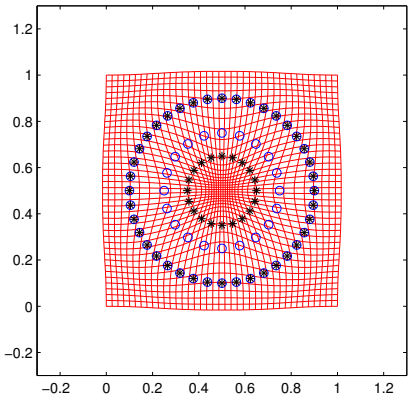

(a) Wendland $\psi_{3,1}$, $c = 0.4$

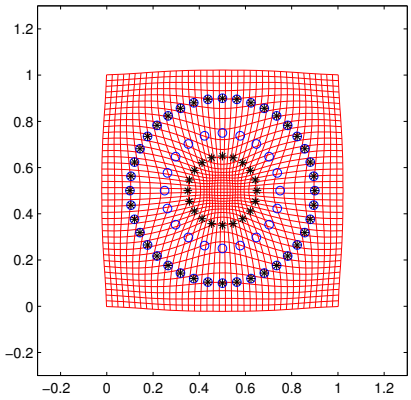

(b) Gneiting $\tau_{2,5}$, $c = 0.7$

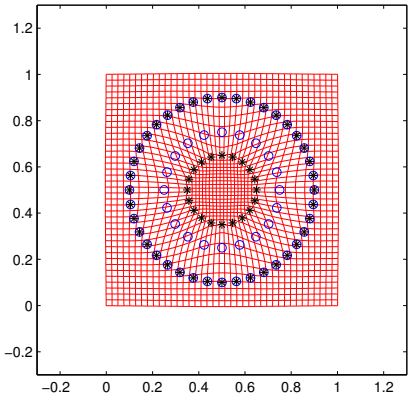

(c) Matérn $M_{1/2}$, $c = 0.1$

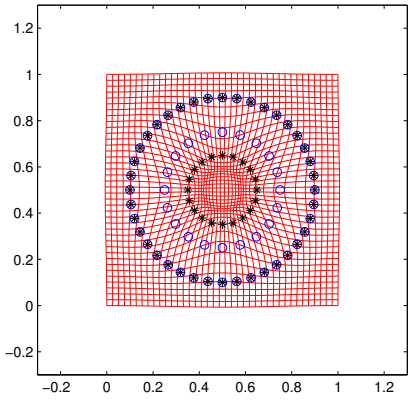

(d) Matérn $M_{5/2}$, $c = 0.04$

Figure 11: Deformation results of circle contraction; the source landmarks are marked by a circle ($\circ$), while the target ones by a star ($*$).

negative points is very small. In four landmarks case, a large value of c must be chosen to obtain a smooth deformation. In this case, $M_{1/2}$ has the best performance. In the second part of the paper, we analyzed the performances of these RBFs in some test cases involving a large number of landmarks. The appropriate c is chosen, also considering the analysis of the parameters done in topology preservation study. Numerical experiments show again that $M_{1/2}$ gives the best registration results among Matérn functions. Also Gneiting functions with large shape parameters can perform well but deformations sometimes significantly affect the trasformed image. These deformations are localized perhaps because of the oscillating behaviours of such functions. However, we can state that for all RBFs we obtain similar and quite low RMSEs. Finally, results deriving from test cases are confirmed in this medical MRI application. This real situation shows applicability of the schemes analyzed in the paper.

Acknowledgements

This work was partially supported by the 2016-2017 projects "Metodi numerici e computazionali per le scienze applicate" and "Approssimazione multivariata e algoritmi efficienti con applicazioni a problemi algebrici, differenziali e integrali" of the Department of Mathematics of the University of Torino. Moreover, the authors acknowledge

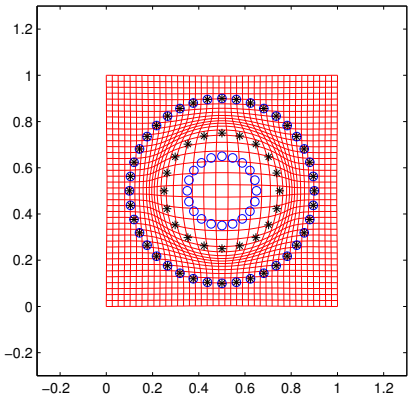

(a) Wendland $\psi_{3,1}$, $c = 0.4$

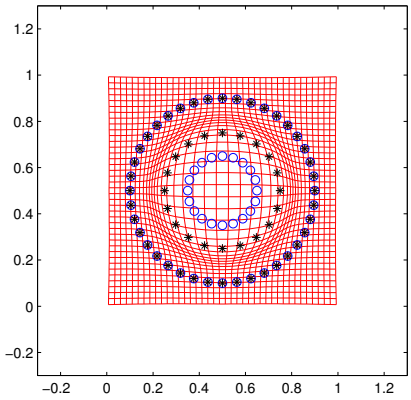

(b) Gneiting $\tau_{2,7/2}$, $c = 0.55$

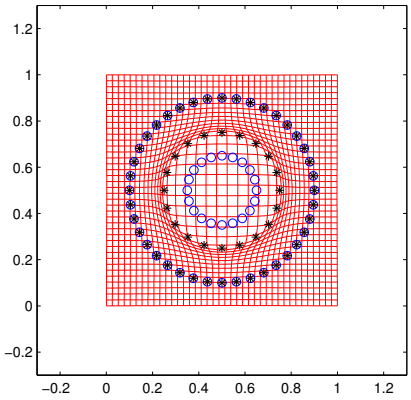

(c) Matérn $M_{1/2}$, $c = 0.1$

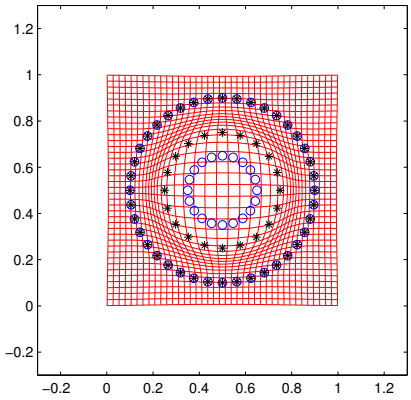

(d) Matérn $M_{3/2}$, $c = 0.083$

Figure 12: Deformation results of circle expansion; the source landmarks are marked by a circle ($\circ$), while the target ones by a star ($*$).

financial support from the GNCS–INdAM. This research has been accomplished within the RITA "Research ITalian network on Approximation".

References

[1] G. Allasia, R. Cavoretto, A. De Rossi, A class of spline functions for landmark-based image registration, Math. Methods Appl. Sci. 35 (2012) 923–934.

[2] G. Allasia, R. Cavoretto, A. De Rossi, Local interpolation schemes for landmark-based image registration: A comparison, Math. Comput. Simulation 106 (2014) 1–25.

[3] G. Allasia, R. Cavoretto, A. De Rossi, B. Quatember, W. Recheis, M. Mayr, S. Demertzis, Radial basis functions and splines for landmark-based registration of medical images, in: T. E. Simos, G. Psihoyios, C. Tsitouras (eds.), Proceedings of the ICNAAM 2010, vol. 1281, AIP Conference Proceedings, 2010, pp. 716–719.

[4] D. S. S. Bedi, M. J. Agarwal, P. Agarwal, Image fusion techniques and quality assessment parameters for clinical diagnosis: a review, International Journal of Advanced Research in Computer and Communication Engineering 2 (2) (2013) 1153–1157.

[5] C. Bosica, R. Cavoretto, A. De Rossi, H. Qiao, On the topology preservation of Gneiting's functions in image registration, Signal Image Video Process. 11 (2017) 953–960.

[6] L. G. Brown, A survey of image registration techniques, ACM Comput. Surveys 24 (4) (1992) 325–376.

[7] M. D. Buhmann, Radial Basis Functions: Theory and Implementation, vol. 12 of Cambridge Monogr. Appl. Comput. Math., Cambridge Univ. Press, Cambridge, 2003.
[8] R. Cavoretto, A. De Rossi, Landmark-based image registration using Gneiting's compactly supported functions, in: T. E. Simos, G. Psihoyios, C. Tsitouras, Z. Anastassi (eds.), Proceedings of the ICNAAM 2012, vol. 1479, AIP Conference Proceedings, 2012, pp. 1335–1338.
[9] R. Cavoretto, A. De Rossi, Analysis of compactly supported transformations for landmark-based image registration, Appl. Math. Inf. Sci. 7 (2013) 2113–2121.
[10] R. Cavoretto, A. De Rossi, H. Qiao, B. Quatember, W. Recheis, M. Mayr, Computing topology preservation of RBF transformations for landmark-based image registration, in: J.-D. Boissonnat et al. (ed.), Curves and Surfaces 2014, vol. 9213 of LNCS, Springer International Publishing, 2015, pp. 96–108.
[11] S. Dawn, V. Saxena, B. Sharma, Remote sensing image registration techniques: a survey, Image and Signal Processing, Lecture Notes in Computer Science 6134 (2010) 103–112.
[12] A. Dogra, M. S. Patterh, CT and MRI brain images registration for clinical applications, J. Cancer Sci. Therapy 6 (1) (2014) 18–26.
[13] G. E. Fasshauer, Meshfree Approximation Methods with MATLAB, World Scientific Publishers, Singapore, 2007.
[14] G. E. Fasshauer, Positive definite kernels: past, present and future, Dolomites Res. Notes Approx. 4 (2011) 21–63.
[15] L. M. G. Fonseca, B. S. Manjunath, Registration techniques for multisensor remotely sensed imagery, Photogrammetric Engineering and Remote Sensing 62 (9) (1996) 1049–1056.
[16] M. Fornefett, K. Rohr, H. S. Stiehl, Radial basis functions with compact support for elastic registration of medical images, Image Vision Comput. 19 (2001) 87–96.
[17] J. Gneiting, Compactly supported correlation functions, J. Multivariate Anal. 83 (2) (2002) 493–508.
[18] J. Gneiting, W. Kleiber, M. Schlather, Matérn cross-covariance functions for multivariate random fields, J. Amer. Statist. Assoc. 105 (491) (2010) 1167–1177.
[19] M. Hasan, X. P. Jia, A. Robles-Kelly, J. Zhou, M. R. Pickering, Multi-spectral remote sensing image registration via spatial relationship analysis on sift keypoints, in: Geoscience and Remote Sensing Sympasium (IGARSS), IEEE, 2010, pp. 1011–1014.
[20] J. P. Heather, M. I. Smith, Multimodal image registration with applications to image fusion, in: 7th IEEE International Conference on Information Fusion, vol. 1, IEEE, 2005, pp. 372–379.
[21] K. P. Indira, D. R. R. Hemamalini, Analysis on image fusion techniques for medical applications, International Journal of Advanced Research in Electrical, Electronics and Instrumentation Engineering 3 (9) (2014) 12051–12057.
[22] J. Kohlrausch, K. Rohr, H. Stiehl, A new class of elastic body splines for nonrigid registration of medical images, J. Math. Imaging and Vision 23 (2005) 253–280.
[23] P. Kostelec, S. Periaswamy, Image Registration for MRI, vol. 46, MSRI Publications, 2003.
[24] J. B. A. Maintz, M. A. Viergever, A survey of medical image registration, Medical Image Analysis 2 (1) (1998) 1–36.
[25] B. Matérn, Spatial Variation, vol. 36 of Lecture Notes in Statistic, Springer-Verlag, Berlin, 1986.
[26] G. K. Matsopoulos, Medical image registration and fusion techniques, Advanced Signal Processing Theory and Implementation for Sonar, Radar, and Non-Invasive Medical Diagnostic Systems, Second Edition, 2009.
[27] T. McInerney, D. Terzopoulos, Deformable models in medical image analysis: a survey, Medical Image Analysis 1 (2) (1996) 91–108.
[28] J. Modersitzki, Numerical Methods for Image Registration, Oxford Univ. Press, Oxford, 2004.
[29] F. P. M. Oliveira, J. M. R. S. Tavares, Medical image registration: a review, Comput. Meth. Biomech. Biomed. Eng. 17 (2) (2014) 73–93.
[30] B. Quatember, M. Mayr, W. Recheis, S. Demertzis, G. Allasia, A. De Rossi, R. Cavoretto, E. Venturino, Development of an accurate method for motion analyses of the heart wall based on medical imagery, in: R. Moreno-Díaz, F. Pichler, A. Quesada-Arencibia (eds.), Computer Aided Systems Theory - EUROCAST 2011, vol. 6928 of LNCS, Springer-Verlag, 2012, pp. 248–255.
[31] B. Quatember, M. Mayr, W. Recheis, S. Demertzis, G. Allasia, A. D. Rossi, R. Cavoretto, E. Venturino, Geometric modelling and motion analysis of the epicardial surface of the heart, Math. Comput. Simulation 81 (2010) 608–622.
[32] K. Rohr, Landmark-Based Image Analysis, Using Geometric and Intensity Models, Kluwer Academic Publishers, MA, Norwell, 2001.
[33] O. Scherzer, Mathematical Models for Registration and Applications to Medical Imaging, Springer, New York, 2006.
[34] M. L. Stein, Interpolation of spatial data: some theory for Kriging, Springer-Verlag, New York, 1999.
[35] P. A. van den Elsen, J. B. A. Maintz, E. J. D. Pol, M. A. Viergever, Automatic registration of CT and MR brain images using correlation of geometrical features, IEEE Trans. Med.l Imag. 14 (1995) 384–395.
[36] H. Wendland, Scattered Data Approximation, vol. 17 of Cambridge Monogr. Appl. Comput. Math., Cambridge Univ. Press, Cambridge, 2005.
[37] X. Yang, Z. Xue, X. Liu, D. R. Xiong, Topology preservation evaluation of compact-support radial basis functions for image registration, Pattern Recognition Lett. 32 (2011) 1162–1177.
[38] B. Zitová, J. Flusser, Image registration methods: a survey, Image Vision Comput. 21 (2003) 977–1000.

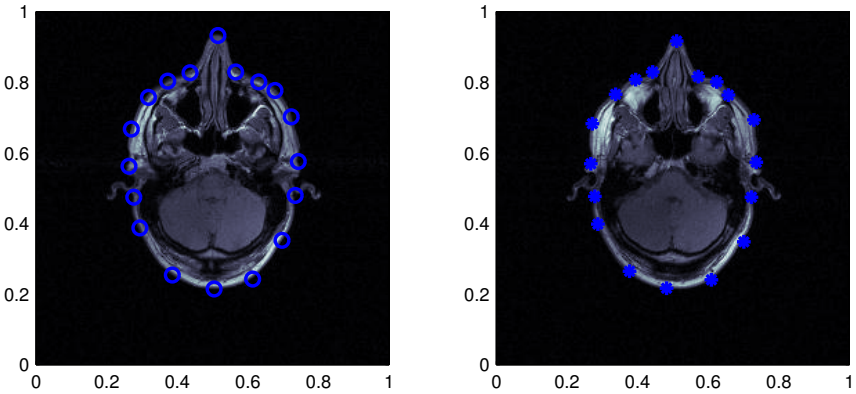

(a) Source image

(b) Target image

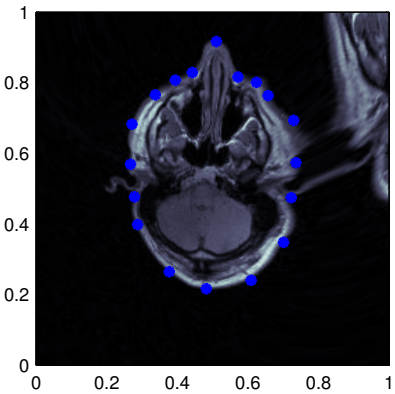

(c) $\psi_{3,1}$, $c = 2$

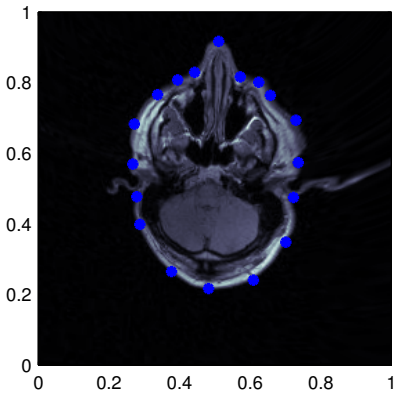

(d) $\tau_{2,7/2}$, $c = 5$

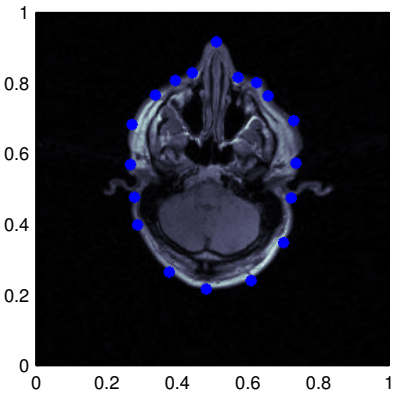

(e) $M_{3/2}$, $c = 2$

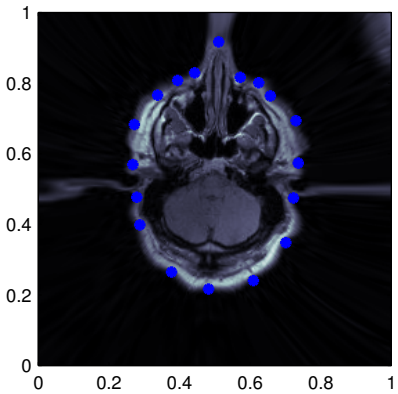

(f) $M_{1/2}$, $c = 5$

Figure 13: The two MRI brain images with related landmarks are given in (a) and (b); registration results are from (c) to (f). The source landmarks are marked by a circle ($\circ$), while the target ones by a star ($*$).